ACS OMEGA

http://pubs.acs.org/journal/acsodf

Article

Formation and Segregation of a Pd−MgO Solid Solution Studied by X-ray Absorption Spectroscopy

Kazu Okumura,* Sachiko Morita, Hikaru Iiyoshi, and Hiromitsu Takaba

Cite This: *ACS Omega* 2023, 8, 7507−7516

Read Online

ACCESS | Metrics & More | Article Recommendations | Supporting Information

ABSTRACT: Thermal treatment of Pd nanoparticles or $Pd(NH_3)_4(NO_3)_2$ supported on MgO resulted in the formation of a solid solution of Pd−MgO, as evidenced by Pd K-edge X-ray absorption fine structure (XAFS). The valence of Pd in the Pd−MgO solid solution was determined to be 4+ from the comparison of X-ray absorption near edge structure (XANES) with reference compounds. A characteristic shrinkage of the Pd−O bond distance was observed in comparison with that of the nearest-neighboring Mg−O bond in MgO, which agreed with the density functional theory (DFT) calculations. The two-spike pattern was observed in the dispersion of Pd−MgO owing to the formation and successive segregation of solid solutions above 1073 K.

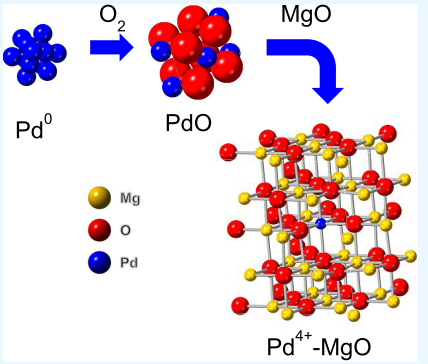

1. INTRODUCTION

Supported Pd catalysts are widely used in fine chemical synthesis,[1] combustion of hydrocarbons such as methane,[2] and NO_x abatement,[3] and the demand for Pd catalysts is increasing progressively. Generally, it is desirable to support Pd in a highly dispersed manner to enhance the surface area on supports. However, the highly dispersed Pd particles often aggregate at high temperatures through sintering in the gas phase, or agglomerate through dissolution and subsequent precipitation in the liquid phase, which results in an irreversible deactivation of Pd. One of the possible methods to keep the highly dispersed Pd form is to make use of the strong interactions between the Pd and the oxide support. Such an interaction was utilized to redisperse the aggregated Pd to regenerate the active species in zeolites.[4] Among the strong interaction between support and Pd, making a solid solution is a promising way for the formation of highly active catalysts, as reported for Pd−CeO_2 catalysts used in CO oxidation or NO reduction,[5] and the Pd perovskite applied to the NO_x reduction.[6] The Pd−CeO_2 solid solution has also been studied in view of the crystal growth suppression of Pd.[7] However, little is known about the interaction between Pd and MgO, particularly for the formation of solid solutions despite the remarkable versatility of Pd/MgO catalysts. For example, nanocrystalline Pd^0 supported on MgO was found to be active in various kinds of organic reactions,[8] including the *N*-monoalkylation of amines with alcohols[9] and Suzuki coupling using chlorobenzene derivatives as the substrate.[10] Pd/MgO was applied to the gas phase reaction as well such as the NO−CO reaction[11] and the hydronation of phenol.[12] Pd/MgO has also been studied from the viewpoint of surface science, in particular the interaction between Pd and the MgO (001) facet.[13] Another example is the study on the growth of Pd particles using a transmission electron microscope (TEM).[14] Not only Pd/MgO but also a Pd/MgO-derived catalyst such as Pd/MgO/SiO_2 has been extensively studied in the methyl isobutyl ketone formation from acetone,[15] CO_2 methanation with hydrogen, and CH_4 reformation.[16]

To investigate the formation process of Pd−MgO solid solutions, poly(vinylpyrrolidone) (PVP) polymer-protected Pd nanoparticles (NPs) were employed as the precursor for Pd to obtain insights into the origin of the interaction between Pd and MgO here. The characteristics of the polymer-protected Pd^0 NPs are their narrow size distribution and high activity in catalytic reactions.[17] Tetraamminepalladium(II) nitrate ($Pd(NH_3)_4(NO_3)_2$) was employed as another Pd precursor to reveal the influence of the precursor type on the formation process of Pd−MgO solid solutions. The MgO support loaded with Pd-NPs and $Pd(NH_3)_4(NO_3)_2$ are denoted as Pd-NP/MgO and $Pd(NH_3)_4(NO_3)_2$/MgO, respectively. The electronic state and local structure of Pd in these samples were analyzed primarily by X-ray absorption fine structure spectroscopy (XAFS), which is a powerful technique to monitor the oxidation states and local structure of Pd even with the low-Pd-loading samples as used here (0.2 wt %).[18]

Received: October 13, 2022
Accepted: January 24, 2023
Published: February 16, 2023

2. EXPERIMENTAL SECTION

2.1. Sample Preparation. A 20% ethanol/water suspension of PVP-protected Pd-NPs (Wako Chemical Co., Renaissance Energy Research Co.) mixed with MgO (JRC-MGO-4, 500A) was evaporated using an evaporator at 300 K. The obtained solid was crushed with a mortar, followed by thermal treatment in the air at 673−1373 K for 3 h in an electric furnace. The PVP-protected Pd-NPs were also loaded on Al_2O_3 (JRC-ALO-7) and SiO_2 (Fuji Silysia Co., Q-10) using similar procedures as well. MgO and Al_2O_3 were obtained from the Catalysis Society of Japan. The loading of Pd was 0.2 wt % unless otherwise stated. $Pd(NH_3)_4(NO_3)_2$ (Wako Chemical Co., 0.2 wt %) was impregnated on MgO from the aqueous solution of the Pd ammine complex in boiling water. The obtained powder was thermally treated in the air in the same way as that used for preparing Pd-NP/MgO.

2.2. Pd K-Edge XAFS Measurements and Analyses. The Pd K-edge XAFS data of Pd-NP- and $Pd(NH_3)_4(NO_3)_2$-loaded supports were collected using synchrotron radiation. The XAFS data were recorded at the NW10A beamline with the approval of the Photon Factory of the High Energy Accelerator Research Organization (KEK-PF-AR, Proposal Nos. 2020G621 and 2022G581). The data were collected with the step scan mode within 30 min using a Si(311) monochromator. The beam size at the sample position was 2.0 mm (horizontal) × 0.8 mm (vertical). For the Pd K-edge extended X-ray absorption fine structure (EXAFS) analysis, the oscillations were extracted using a spline smoothing method. The Fourier transform (FT) of the k^3-weighted EXAFS oscillations and $k^3\chi(k)$ from k-space to r-space was conducted in the range of 2.5−14 $Å^{-1}$ for curve fitting analysis for thermally treated samples in the air. The curve fitting analysis was conducted in 1−3 Å the in r-space. The Fourier transform (FT) of the k^3-weighted EXAFS oscillations and $k^3\chi(k)$ from k-space to r-space was conducted in the range of 2.5−15 $Å^{-1}$ for the samples obtained after temperature-programmed reduction in hydrogen (H_2-TPR). We confirmed that the number of independent parameters satisfied the criteria for analysis $\left(N = \frac{2\Delta r \Delta k}{\pi}\right)$. The EXAFS data were analyzed using the REX software (Rigaku Co.) with curve fitting employing the EXAFS data of PdO and Pd foil to analyze the Pd−O and Pd−Pd bonds, respectively. For the analysis of the Pd−Mg bond, parameters were obtained using the FEFF8.0 program from the University of Washington.[19] The parameters (i.e., coordination number (CN), bond distance, ΔE_0, Debye−Waller factor) were not fixed (floating).

2.3. Physicochemical Characterization Other than XAFS. N_2 adsorption isotherms were recorded on a BELSORP mini X (Microtrac Bel Co.) instrument. The samples were dehydrated in a vacuum at 573 K prior to the N_2 adsorption measurements to obtain the isotherm data. The TEM images of the Pd−MgO samples were obtained using a JEOL-JEM-2100 microscope. Briefly, an ethanol suspension of the sample was dropped onto Cu grids coated with a C-coated porous thin membrane (NEM, Japan) and dried. Thereafter, TEM observations were performed at an operating voltage of 200 kV. The X-ray diffraction (XRD) patterns of the powders were obtained under ambient conditions using a MiniFlex X-ray diffractometer (Rigaku Co.) using Cu Kα radiation in the 2θ range from 20 to 90°. The scanning speed for the collection of XRD data was 1°/min. The dispersion of Pd on the supports was evaluated using the BELCAT II equipment (Microtrac BEL Co.). The samples were treated with H_2 at 773 K for 0.5 h before the measurements. The dispersion value of Pd was measured via CO adsorption at 323 K using a thermocouple detector (TCD), assuming a CO/Pd ratio of 1 for the calculation of dispersion. Further, H_2-TPR was conducted using the same equipment for the analysis of dispersion (BELCAT II). The experiments were performed using 5% H_2/Ar (50 mL/min flow rate) without pretreatment. The samples were heated at a temperature ramp rate of 10 K/min from room temperature to 923 K. A TCD detector was used to monitor the concentration of H_2 in the flowing gas.

2.4. Computer Simulation. Density functional theory (DFT) calculations using the DMol3 program package[20] was carried out to calculate the structure of the Pd−MgO crystal under three-dimensional periodic condition. The physical wave functions were expanded in terms of accurate numerical basis sets. A double numerical plus d-functions was used for all calculations, employing the generalized gradient approximation functional developed by Perdew−Burke−Ernzerhof.[21] Core electrons were treated by effective core potentials. The convergence tolerances for energy, maximum force, and maximum displacement were less than 2.0 × 10^{-5} Ha, 0.004 Ha/Å, and 0.005 Ha/Å, respectively. The K-point was set to 2 × 2 × 2. A unit cell consists of $Pd_1Mg_{30}O_{32}$, where the two nearest Mg atoms were deleted from the perfect crystal of $Mg_{32}O_{32}$ and a deleted Mg atom was substituted with a Pd atom to maintain a neutral charge. The cell parameter of the cubic unit cell was a = 8.42240 Å, which is the same as that for a perfect crystal MgO. We found that the cell parameter is slightly increased after the optimization of cell parameters using DFT; however, the change of the cell parameter would be smaller if we consider random substitution with a larger unit cell. Therefore, in the following DFT calculations, the unit cell parameter was fixed to those for the original MgO crystal parameters.

3. RESULTS AND DISCUSSION

3.1. Pd K-Edge EXAFS Studies. Figures 1a and S1a show the radial distribution functions (i.e., FTs) and $k^3\chi(k)$ data of the Pd K-edge EXAFS data of Pd-NPs supported on different types of supports and thermally treated at 1073 K, respectively. The data obtained by the curve fitting analysis for Pd/MgO are listed in Table 1. The simulated EXAFS oscillations are shown

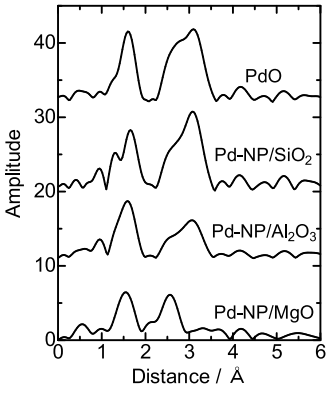

Figure 1. Pd K-edge EXAFS distribution functions (EXAFS-FT) of pristine PdO and Pd-NPs loaded on MgO, Al_2O_3, and SiO_2 and heat-treated at 1073 K. Fourier transform range: 3−15 $Å^{-1}$.

https://doi.org/10.1021/acsomega.2c06604
ACS Omega 2023, 8, 7507−7516

Table 1. Curve Fitting Analysis of Pd K-Edge EXAFS Data Measured at Room Temperature for Pd-NP and $Pd(NH_3)_4(NO_3)_2$ Loaded on MgO Treated at 1073 K in the Air

sample	scatterer	CN[a]	R (Å)[b]	ΔE_0 (eV)[c]	DW (Å)[d]	R_f (%)[e]
Pd-NP/MgO	O	4.7 ± 1.0	2.04 ± 0.01	−6 ± 3	0.078 ± 0.022	3.2
	Mg	5.1 ± 0.9	2.99 ± 0.01	−4 ± 2	0.069 ± 0.022	
$Pd(NH_3)_4(NO_3)_2$/MgO	O	7.5 ± 1.0	2.05 ± 0.01	−1 ± 4	0.115 ± 0.026	2.1
	Mg	6.5 ± 1.2	2.98 ± 0.01	2 ± 2	0.071 ± 0.023	
MgO[f]	O	(6)	(2.11)			
	Mg	(12)	(3.01)			

[a]coordination number. [b]bond distance. [c]difference in the origin of photoelectron energy between the reference and the sample. [d]Debye−Waller factor. [e]residual factor. [f]data of X-ray crystallography. Fourier transform range: 2.5−14 $Å^{-1}$. Fourier filtering range: 1−3 Å.

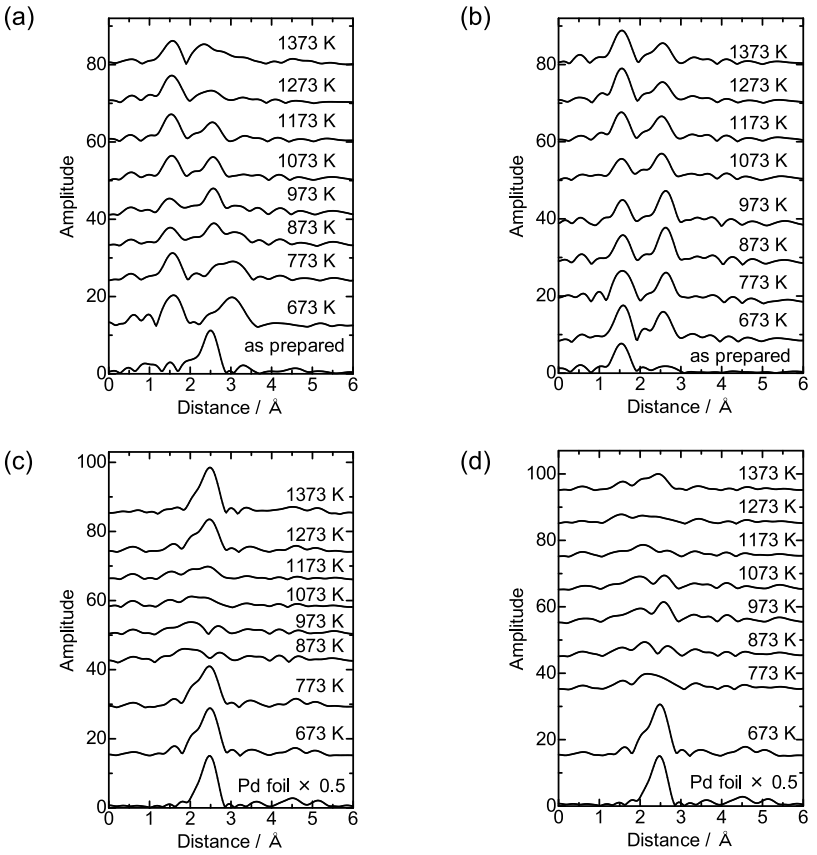

Figure 2. Pd K-edge EXAFS distribution functions (EXAFS-FT) of (a) Pd-NP/MgO, (b) $Pd(NH_3)_4(NO_3)_2$/MgO treated at different temperatures and (c) Pd-NP/MgO, (d) $Pd(NH_3)_4(NO_3)_2$/MgO treated at different temperatures, followed by H_2-TPR up to 923 K. Fourier transform range: 3−15 $Å^{-1}$.

in Figure S2a. EXAFS-FT of Pd-NP/SiO_2 agreed well with that of PdO in which Pd−O and Pd−(O)−Pd bonds appeared to be around 1.1−2.0 and 2.3−3.6 Å, respectively, indicating that the simple oxidation of Pd^0 and the formation of the aggregated PdO progressed on SiO_2. The Pd−(O)−Pd peak splits because of the presence of overlapping bonds at 3.10 (CN = 4) and 3.49 Å (CN = 8). The intensity of the Pd−(O)−Pd bond of Pd/Al_2O_3 was slightly lower than those of PdO. The difference suggested that the partial dispersion of PdO occurred on Al_2O_3. In the case of Pd-NP/MgO, two peaks appeared at 1.7 and 2.7 Å (phase shift uncorrected); the feature was much different from those of Pd-NP/Al_2O_3 and Pd-NP/SiO_2. The first shell could be straightforwardly assigned to the Pd−O bond from comparison with the spectrum of the PdO reference. The second peak appearing at 2.7 Å was assigned to the Pd−Mg bond according to the curve fitting analysis. The bond distance of the Pd−Mg peak was calculated to be 2.99 ± 0.01 Å, which agreed with that of the nearest-neighboring Mg−Mg (3.01 Å) bond in MgO. The possibility of the formation of the spinel oxide (Mg_2PdO_4) may be excluded because the bond distance of the nearest-neighboring Pd−Mg distance was much longer in Mg_2PdO_4 (3.48 Å) than that (3.01 Å) in the MgO crystal.[22] Furthermore, no diffraction assignable to crystalline phases other than MgO was found in the XRD pattern of Pd-NP/MgO treated at 1073 K, as will be discussed later. The CN of the Pd−Mg bond was calculated to be 5.1 ± 0.9; the value was much smaller than that of the nearest-neighboring Mg−Mg bond (CN = 12). The CN of the Pd−O bonds was calculated to be 4.7 ± 1.0, which was smaller than that of the nearest-neighboring Mg−O bond of MgO (CN = 6) as well. The reason may be that the Pd ions in the solid solution were located close to the surface of MgO.

https://doi.org/10.1021/acsomega.2c06604
ACS Omega 2023, 8, 7507−7516

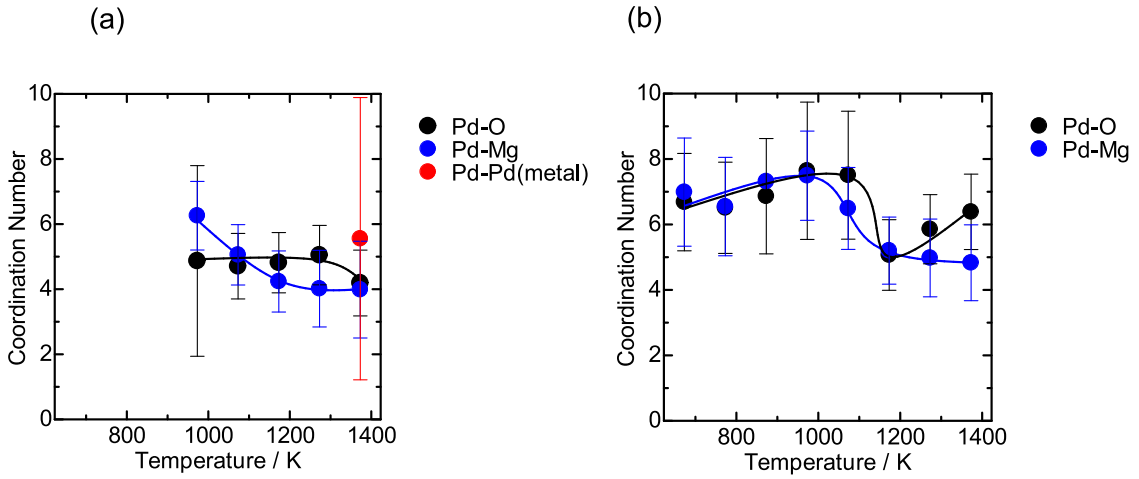

Figure 3. Coordination numbers of Pd−O, Pd−Mg, and Pd−Pd bonds determined by Pd K-edge EXAFS plotted as a function of the thermal treatment temperature for (a) Pd-NP/MgO and (b) $Pd(NH_3)_4(NO_3)_2$/MgO.

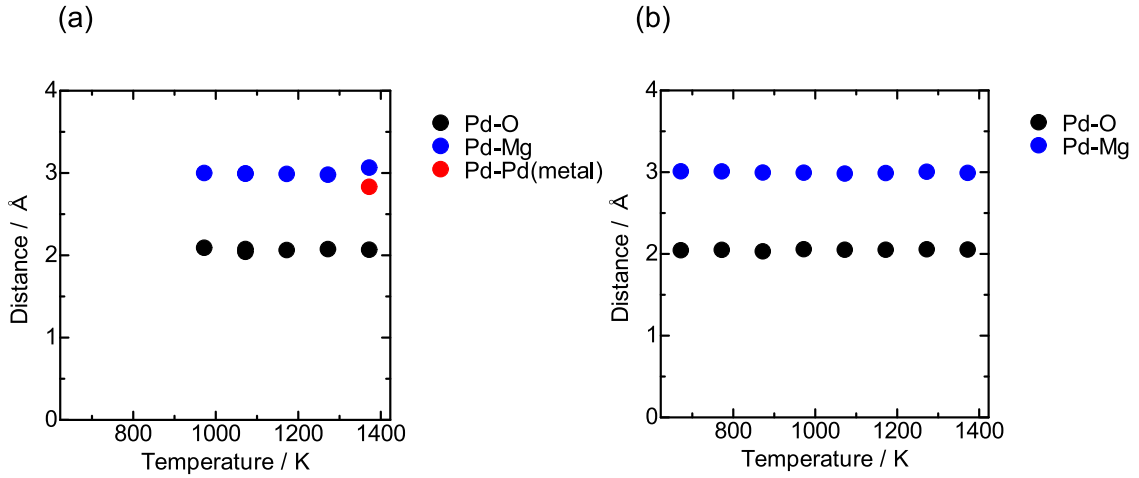

Figure 4. Distances of the Pd−O, Pd−Mg, and Pd−Pd bonds determined by Pd K-edge EXAFS plotted as a function of the thermal treatment temperature for (a) Pd-NP/MgO and (b) $Pd(NH_3)_4(NO_3)_2$/MgO.

Figure S3 shows the EXAFS-FT of Pd-NP/MgO with different Pd loading, which was treated at 1073 K. The EXAFS-FT of the 0.4 wt % Pd samples were close to that of PdO, indicating that the formation of the solid solution hardly occurred, although the intensity of the second shell assignable to Pd−(O)−Pd bonds was slightly lower than that of bulk PdO. In contrast, the formation of the solid solution was found in 0.1 and 0.2 wt % Pd samples. The EXAFS-FT indicated that the formation of the Pd−MgO solid solution occurred in the samples with Pd loading less than 0.2 wt %.

Figure 2a shows the EXAFS-FTs of Pd-NP/MgO treated in the range of 673−1373 K and the as-prepared sample. The corresponding $k^3\chi(k)$ data are provided in Figure S1b. In the EXAFS-FT of the as-prepared sample, the peak assignable to the Pd−Pd bond was observed at 2.6 Å (phase shift uncorrected), suggesting that the metal Pd-NPs loaded on MgO remained almost intact. For the sample heated at 673 K, new peaks assignable to the Pd−O and Pd−(O)−Pd bonds appeared at 1.7 and 3.3 Å (phase shift uncorrected), respectively, as a result of the oxidation of Pd-NPs to form aggregated PdO during thermal treatment in the air. The EXAFS-FTs of the samples heated at 973 and 1073 K were similar; they showed two peaks at 1.7 and 2.7 Å, which were assigned to Pd−O and Pd−Mg bonds, respectively, as already discussed above. The change meant that the Pd−MgO solid solution progressed via the formation of PdO. With a further increase in the thermal treatment temperature to 1373 K, the broad peak corresponding to the second coordination sphere emerged at 2.6 Å (phase shift uncorrected), probably due to the reappearance of metallic Pd−Pd bonds.

Figure 3a shows the CNs of the Pd−O, Pd−Mg, and Pd−Pd (metal) bonds of Pd-NP/MgO plotted as a function of the thermal treatment temperature in the range between 973 and 1373 K. The corresponding Debye−Waller factors are shown in Figure S4. The Pd−Mg and Pd−O bonds appeared above 973 K due to the formation of Pd−MgO solid solutions. When the thermal treatment temperature was increased further from 973 to 1273 K, the CN(Pd−Mg) decreased from 6 to 4, probably due to the migration of Pd ions in the Pd−MgO solid solution to the surface of MgO. The Pd K-edge EXAFS of the Pd−MgO treated at 1373 K was successfully simulated after including the metal Pd−Pd bond in the curve fitting analysis. The appearance of the metal Pd−Pd bond indicated that the Pd−MgO solid solution was no longer stable at 1373 K and that Pd^0 and MgO started to segregate. The reason for the formation of metal Pd may be because the palladium oxide was

https://doi.org/10.1021/acsomega.2c06604
ACS Omega 2023, 8, 7507−7516

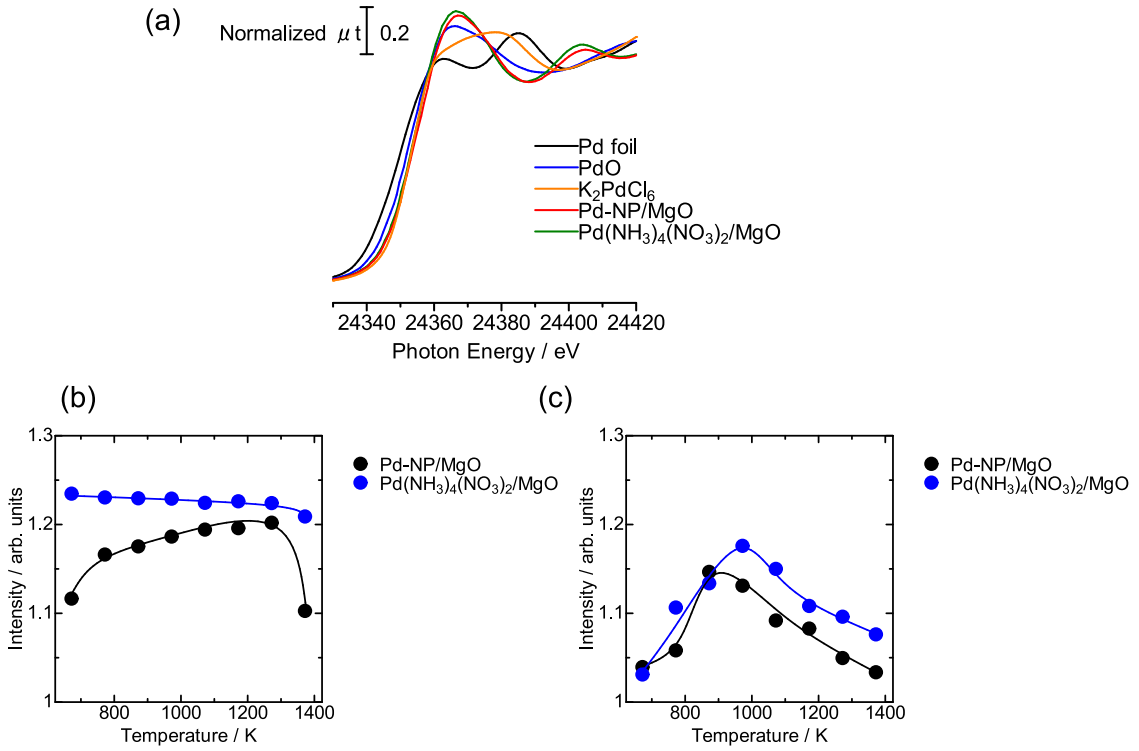

Figure 5. (a) Pd K-edge XANES profiles of Pd-NP/MgO and $Pd(NH_3)_4(NO_3)_2$/MgO treated at 1073 K and reference compounds. The intensity of white lines of Pd K-edge XANES plotted as a function of the thermal treatment temperature for (b) Pd-NP/MgO and $Pd(NH_3)_4(NO_3)_2$/MgO and (c) Pd-NP/MgO and $Pd(NH_3)_4(NO_3)_2$/MgO measured after H_2-TPR.

thermodynamically unstable to decompose into metal Pd, while metal Pd was stable form at temperatures higher than 973 K as reported in the literature.[23] Apart from the CNs, the distances of the Pd−O, Pd−Mg, and Pd−Pd (metal) of Pd-NP/MgO are plotted as a function of the thermal treatment temperature in Figure 4a. The Pd−O and Pd−Mg distances were not dependent on the treatment temperature.

Figure 2b shows the EXAFS-FTs of the as-prepared sample and $Pd(NH_3)_4(NO_3)_2$/MgO treated at 673−1373 K. The corresponding $k^3\chi(k)$ data are provided in Figure S1c. In the EXAFS of the as-prepared sample, a single peak assignable to tetracoordinated Pd−N (NH_3) bonds appeared at 1.7 Å (phase shift uncorrected), which arose from the four NH_3 ligands coordinated to the Pd center. The EXAFS-FT and $k^3\chi(k)$ of $Pd(NH_3)_4(NO_3)_2$/MgO treated at 673−1373 K were similar to those of Pd-NP/MgO treated at 973−1073 K. This similarity indicated that a Pd−MgO solid solution already formed at 673 K. The representative curve fitting data of $Pd(NH_3)_4(NO_3)_2$/MgO treated at 1073 K are included in Figure S2b and Table 1. The bond distances in the Pd−MgO solid solution prepared using $Pd(NH_3)_4(NO_3)_2$ as the Pd precursor was close to that of Pd-NP/MgO, for which the distances of Pd−O and Pd−Mg bonds were observed to be 2.05 and 2.98 Å, respectively. The temperature-dependent changes in the CNs are shown in Figure 3b. The maximum CN(Pd−Mg) value (8) was reached at 973 K. The maximum CN(Pd−Mg) value of $Pd(NH_3)_4(NO_3)_2$/MgO (CN = 8) was larger than that of Pd-NP/MgO (CN(Pd−Mg) = 6). This difference suggested that the location of Pd ions was different; in the case of $Pd(NH_3)_4(NO_3)_2$/MgO, Pd ions were located deep inside the crystals of MgO, while in the former case, the Pd cations were located relatively close to the surface of MgO. The use of an aqueous solution in the preparation probably caused the close interaction between Pd and MgO. This is one of the reasons for showing higher CN(Pd−Mg) value of Pd(NH in that complex ($Pd(NH_3)_4(NO_3)_2$/MgO compared with that of Pd-NP/MgO at a given preparation temperature. Another important point is the difference in the temperature at the impregnation procedure: In the case of $Pd(NH_3)_4(NO_3)_2$, the impregnation on MgO was conducted using a water bath with boiling water. The use of boiling water promoted the hydration of MgO, producing Mg(OH) of MgO to give $Mg(OH)_2$ with high surface area, and the intimate interaction between Pd and MgO to form a solid solution within the MgO crystals. As for Pd−O bonds, the CNs of the Pd−O bond was the largest in the temperature range between 873 and 1073 K. The distances of the Pd−O and Pd−Mg bonds of the solid solution of $Pd(NH_3)_4(NO_3)_2$/MgO (Figure 4b) were consistent with those of Pd-NP/MgO (Figure 4a).

Figure 2c shows the Pd K-edge EXAFS-FT of the Pd-NP/MgO measured after the H_2-TPR experiment (up to 923 K), which was treated at different temperatures prior to H_2-TPR. The corresponding $k^3\chi(k)$ data are shown in Figure S5a. The EXAFS of Pd-NP/MgO treated at 673 and 773 K were close to that of Pd foil. The formation of the metal Pd was explained simply as a result of the reduction of loaded PdO with H_2. The metal Pd was observed in the 1273 and 1373 K-treated samples as well. Probably, the formation of metal Pd was caused by the reduction of Pd−MgO solid solutions in which Pd was located close to the surface of MgO. In contrast to these, the Pd−Pd bond of metal Pd was hardly observed in the samples treated at 873−1173 K, meaning the reduction of Pd ions was suppressed in these samples.

Figure 2d shows the Pd K-edge EXAFS-FT of Pd-$(NH_3)_4(NO_3)_2$/MgO measured after the H_2-TPR experiment, which was treated at different temperatures. The correspond-

https://doi.org/10.1021/acsomega.2c06604
ACS Omega 2023, 8, 7507−7516

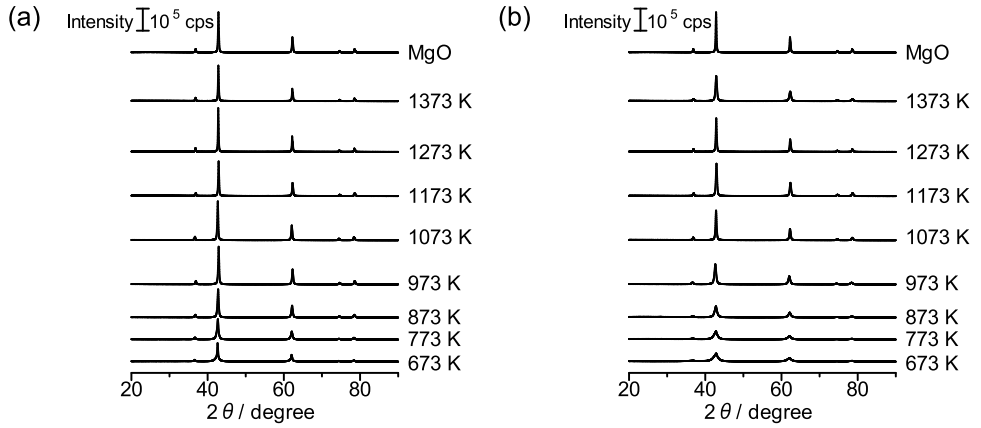

Figure 6. XRD patterns of (a) Pd-NP/MgO and (b) $Pd(NH_3)_4(NO_3)_2$/MgO treated at different temperatures and MgO.

ing $k^3\chi(k)$ data are shown in Figure S5b. In the EXAFS-FT of these samples, the formation of the metal Pd−Pd bond was not clearly observed except for the sample treated at 673 K, indicating that the reduction of the metal cation in Pd−MgO hardly occurred even with the H_2 treatment up to 1373 K. The difference of Pd K-edge EXAFS between Pd-NP/MgO and $Pd(NH_3)_4(NO_3)_2$/MgO suggested that the reduction of Pd was hindered probably because Pd^{4+} ions located inside the crystals of MgO in the latter case.

3.2. Pd K-Edge XANES. Information on the valence and symmetry around a given element could be obtained from X-ray absorption near edge structure (XANES), which is sensitive to long-range order because of the large mean free path of the photoelectron in the energy range of 1−100 eV above the absorption edge.[24] Figure 5a shows the Pd K-edge XANES profiles of Pd-NP/MgO and $Pd(NH_3)_4(NO_3)_2$/MgO treated at 1073 K and reference samples. The formation of the solid solution in the samples treated at 1073 K was confirmed with Pd K-edge EXAFS as described above. The inflection points and the peak top energy of the white line tended to shift to higher energy with an increase in the valence of Pd in the reference compounds (Pd foil, PdO, and K_2PdCl_6), the tendency is consistent with that reported previously.[25] The inflection points of the XANES profile for Pd-NP/MgO agreed with those of K_2PdCl_6 (24352 eV), indicating that the valence of Pd in Pd/MgO was 4+. In agreement with this, the color of the samples was pale pink, which is characteristic of Pd^{4+} as observed with K_2PdCl_6 (Figure S6). The ionic radius of Pd^{4+} has been reported to be 0.625 Å, which is comparable to that of hexacoordinated Mg^{2+} (0.720 Å).[26] Probably, the close value of the ionic radii resulted in the formation of a Pd−MgO solid solution. The difference in the ionic radii is calculated to be 15%, which is within the criteria for the formation of a solid solution (Hume−Rothery's rules[27]). Otto et al. reported that Pd^{4+} exists stably on the catalyst through the interaction with the support based on the X-ray photoelectron spectroscopy analysis.[28] In agreement with these reports, Pd^{4+} may be stabilized with the strong interaction with MgO here. Meanwhile, the peak characteristic of the solid solution appeared in the Pd K XANES profile at 24,404 eV in both Pd-NP/MgO and $Pd(NH_3)_4(NO_3)_2$/MgO (Figure 5a). A similar peak was observed in the XANES of Ni K-edge for NiO−MgO, Co K-edge for CoO-MgO,[29] and Pt L_3-edge of Pt-MgO solid solutions[30] but not for the reference compounds. It should be noted that the intensity of the white line of Pd/MgO was higher than that of PdO and K_2PdCl_6, probably as the result of the Pd−MgO solid solution. The intensity of the white line is plotted as a function of the thermal treatment temperature in Figure 5b. In the case of Pd-NP/MgO, the white line intensity was low at 673 and 1373 K probably due to the formation of PdO and the existence of Pd^0, respectively, while the gradual decrease in the intensity of the white line was observed accompanied by treatment temperature in Pd-$(NH_3)_4(NO_3)_2$/MgO; the change suggested that the gradual segregation progressed accompanied by an increase in the treatment temperature.

Figure 5c shows the intensity of the white line of Pd K-edge XANES for Pd-loaded samples on MgO measured after the H_2-TPR experiment, which will be described later. Both Pd-NP/MgO and $Pd(NH_3)_4(NO_3)_2$/MgO showed a bell-shaped dependence of intensity on the treatment temperature. The change suggested that the reduction of Pd^{4+} was suppressed in the samples treated at 800−1200 K because Pd^{4+} was located beneath the MgO surface, while Pd was located close to the surface of MgO in the sample treated at lower (<800 K) and higher (>1200 K) temperatures so that the reduction of Pd ions was promoted to give Pd^0 in both temperature ranges.

3.3. XRD Pattern, Specific Surface Area, and TEM Study. Figure 6 shows the XRD patterns for Pd-NP/MgO and $Pd(NH_3)_4(NO_3)_2$/MgO treated at different temperatures. The XRD patterns agreed with that of MgO, and no diffraction assignable to crystalline phases including Mg_2PdO_4 spinel and metal Pd other than MgO were found.[31] The feature was different from those of Pd-NP/Al_2O_3 and Pd-NP/SiO_2 treated at 1073 K, in which sharp diffraction assignable to the (101) facet of PdO appeared at 33.8° (Figure S7); the formation of PdO was already confirmed with Pd K-edge EXAFS in these samples.

The specific surface areas calculated from the N_2 adsorption isotherms are shown in Figure 7. The isotherms used for calculation are displayed in Figure S8. The specific surface area of the untreated MgO and Pd-NP/MgO was almost constant in the temperature range of 873−1273 K, while a monotonic decrease in the specific surface area was observed for the boiling water-treated MgO and $Pd(NH_3)_4(NO_3)_2$/MgO. The reason for the higher specific surface of $Pd(NH_3)_4(NO_3)_2$/MgO compared with that of Pd-NP/MgO may be that the former was prepared with evaporation on a boiling water bath, which resulted in the formation of MgO to $Mg(OH)_2$ with high surface area.[32]

The TEM images of untreated and thermally treated Pd-NP/MgO samples are displayed in Figure 8. The TEM image

https://doi.org/10.1021/acsomega.2c06604
ACS Omega 2023, 8, 7507−7516

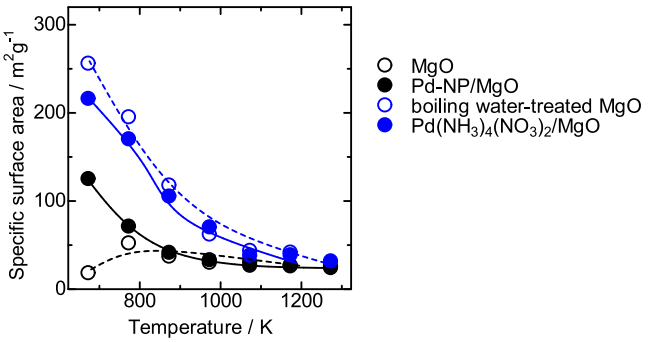

Figure 7. Specific surface are of Pd-NP/MgO and $Pd(NH_3)_4(NO_3)_2$/MgO plotted as a function of the thermal treatment temperature.

of the untreated Pd-NP/MgO sample showed well-dispersed Pd particles of 2−7 nm diameter, while Pd particles could not be found in the TEM image of Pd/MgO thermally treated at 1073 K, probably due to the formation of a Pd−MgO solid solution. Pd nanoparticles were not observed in the TEM image of Pd-NP/MgO even after treatment at 1273 K (Figure 8c), meaning that the highly dispersed Pd was preserved after the treatment at high temperatures.

3.4. H_2-TPR Analysis. Figure 9a,b presents the H_2-TPR plots of Pd-NP/MgO and $Pd(NH_3)_4(NO_3)_2$/MgO thermally treated at different temperatures, together with that of pristine PdO, respectively. The H_2 consumption peak appeared at 340 K in the H_2-TPR of PdO, which could be attributed to the reduction of Pd^{2+} to Pd^0. In the H_2-TPR plots of Pd-NP/MgO treated at 673 K, major reduction peaks appeared at 420 and ca. 610 K, at a temperature much higher than that of PdO, probably due to the strong interaction between Pd and MgO, which retarded the reduction of Pd cations. The intensity of the H_2 consumption peak was small in the samples treated at 873 and 973 K, as a result of the suppression of the reduction of Pd^{4+} because the cations are located inside the MgO crystals as inferred from the Pd K-edge EXAFS analysis. On further increase in the thermal treatment temperature higher than 1073 K, apparent H_2 consumption peaks appeared at 413, 453, and 740 K again. The reappearance may be caused by the migration of Pd^{4+} to the surface of MgO, which facilitated the reduction of Pd^{4+} to Pd^0 with H_2. In the H_2-TPR profiles of $Pd(NH_3)_4(NO_3)_2$/MgO (Figure 9b), the evolution of the H_2 consumption peaks was not apparent except for the samples treated at 673 and 1373 K, meaning that the overall reduction of Pd cations was suppressed compared with that of Pd-NP/MgO. The difficulty of the reduction with H_2 in Pd-$(NH_3)_4(NO_3)_2$/MgO may be caused because the Pd^{4+} cations are located deep inside the MgO compared with that of Pd^{4+} in Pd-NP/MgO as suggested by the Pd K-edge EXAFS analysis. Such a shift was previously observed for Pd/CeO_2, in which oxidized Pd species strongly interacted with the CeO_2 support.[33]

3.5. Dispersion of Pd Measured with CO Adsorption. Figure 10 shows the dispersion values of Pd in Pd-NP/MgO and $Pd(NH_3)_4(NO_3)_2$/MgO plotted as a function of the thermal treatment temperature. In the case of Pd-NP/MgO, the dispersion of Pd decreased to 2% at 973 K accompanied by an increase in the temperature. Further increase in the treatment temperature resulted in an increase in the dispersion; the second peak appeared at 1173 K, at which the dispersion reached 28%. Probably, the migration of Pd^{4+} to the MgO surface resulted in the reduction of Pd^{4+} to Pd^0 so that the adsorption of CO was promoted in the sample treated at 1173 K. The conjecture was supported by the Pd K-edge EXAFS and H_2-TPR measurements. The dispersion dependence of $Pd(NH_3)_4(NO_3)_2$/MgO on the treatment temperature was similar to that of Pd-NP/MgO, while the maximum dispersion of the former was smaller than that of the latter, probably because the Pd^{4+} cations were located deep inside the MgO, which resulted in the incomplete reduction of the Pd cation to form Pd^0 as supported by the CNs change in EXAFS data (Figure 3d).

3.6. DFT Simulation. The structure of the Pd−MgO solid solution was simulated by calculations after two Mg^{2+} ions in the MgO lattice were replaced with one Pd^{4+} ion. The location of Pd^{4+} in the MgO crystal did not change after the replacement of Mg^{2+} with Pd^{4+} as shown in Figure 11. The binding energies of PdO_2 in the Pd−MgO solid solution and PdO were calculated to be −232.0943 and −183.7925 kcal/mol, respectively (Figure S9). This means that the Pd^{4+} in Pd−MgO is more stable than the Pd^{2+} in bulk PdO. The distance of the mean nearest-neighboring Mg−O bond was calculated to be 2.06 Å (Figure S10 and Table S1), which was almost consistent with that obtained with the EXAFS analysis (2.04 Å). The distance was shorter than that of Mg−O in the MgO crystal (2.106 Å); a characteristic shrinkage of the Pd−O distance compared with the Mg−O bond was found in the

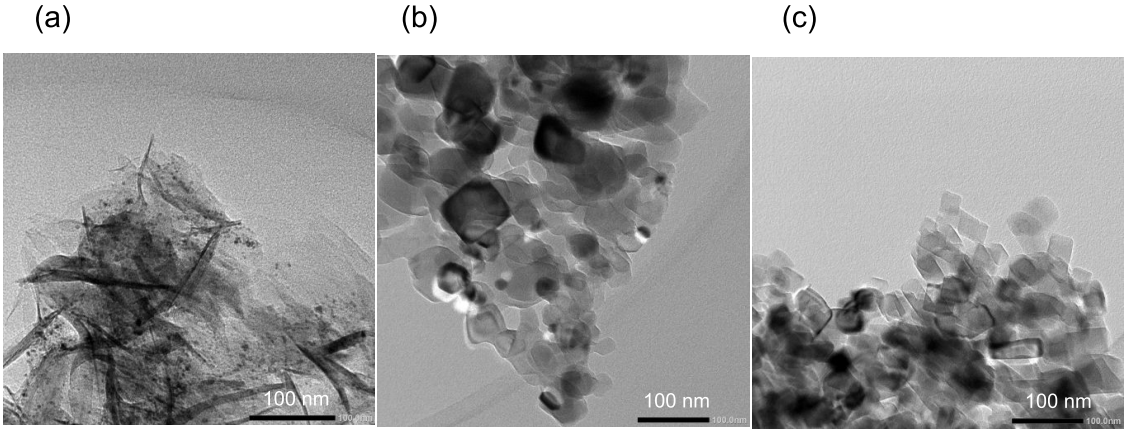

Figure 8. TEM images of Pd-NP/MgO: (a) the as-prepared sample, (b) the sample thermally treated at 1073 K, and (c) the sample thermally treated at 1273 K.

https://doi.org/10.1021/acsomega.2c06604
ACS Omega 2023, 8, 7507−7516

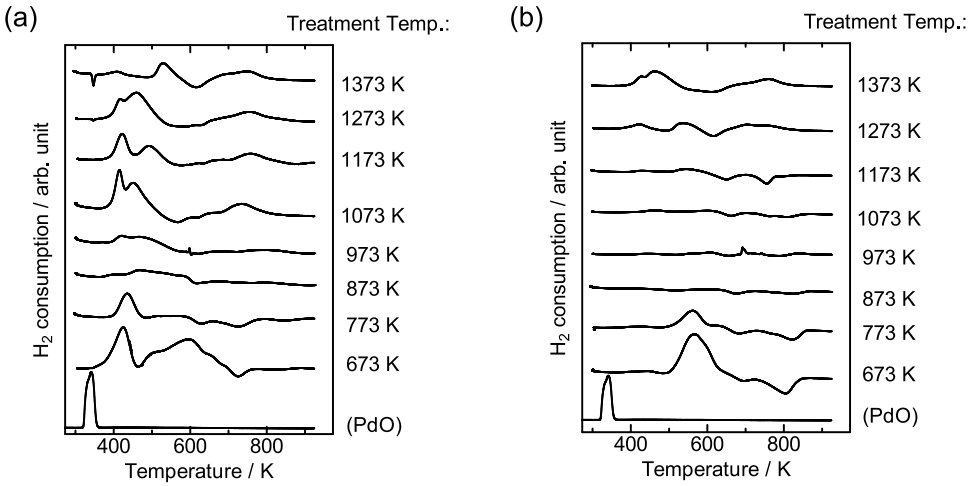

Figure 9. H_2-TPR profiles of (a) Pd-NP/MgO, (b) $Pd(NH_3)_4(NO_3)_2$/MgO treated at different temperatures, and pristine PdO.

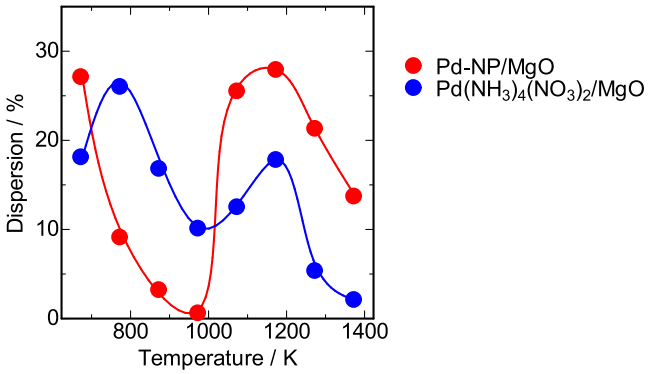

Figure 10. Dependence of the dispersion of Pd in Pd-NP/MgO and $Pd(NH_3)_4(NO_3)_2$/MgO on the thermal treatment temperature.

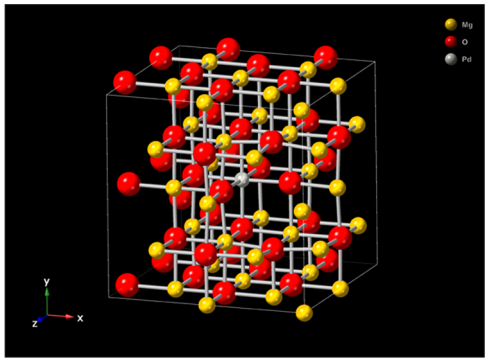

Figure 11. Optimum structure of Pd−MgO solid solutions ($Pd_1Mg_{30}O_{32}$) calculated with DFT.

solid solution. The reason for the shorter Pd^{4+}−O^{2-} bond distance compared with that of Mg−O may be ascribed to the difference in valences. Namely, the Pd^{4+} cation with a higher valence (4+) than that of Mg^{2+} (2+) attracted the O^{2-} anion. On the other hand, the nearest-neighboring Pd−Mg distance in the Pd−MgO solid solutions was close to that of the Mg−Mg bond in MgO (3.00 ± 0.03 Å, Figure S11), which was consistent with the EXAFS data (Table 1).

4. CONCLUSIONS

The formation and segregation processes of a Pd−MgO solid solution were analyzed in detail using Pd K-edge XAFS coupled with other physicochemical techniques. The temperature for the complete formation of a Pd−MgO solid solution was observed to be in the range of 973−1273 and 673−1373 K when Pd-NPs and $Pd(NH_3)_4(NO_3)_2$ were employed as Pd precursors, respectively. In the former case, the formation of the solid solution progressed via PdO from Pd^0, while the thermal treatment of the Pd−MgO solid solution at 1373 K resulted in the partial segregation of Pd and MgO again, which resulted in the second peak at 1173 K in dispersion measurements. The behavior of Pd indicated that the location of Pd changed significantly depending on the thermal treatment temperature.

■ ASSOCIATED CONTENT

Supporting Information

The Supporting Information is available free of charge at https://pubs.acs.org/doi/10.1021/acsomega.2c06604.

EXAFS and XANES; XRD patterns; N_2 adsorption isotherms, and DFT optimized crystal structure and bond distances (PDF)

■ AUTHOR INFORMATION

Corresponding Author

Kazu Okumura − *Department of Applied Chemistry, School of Advanced Engineering, Kogakuin University, Hachioji 192-0015 Tokyo, Japan*; orcid.org/0000-0002-7952-3482; Email: okmr@cc.kogakuin.ac.jp; Fax: +81-42-628-4508

Authors

Sachiko Morita − *Department of Applied Chemistry, School of Advanced Engineering, Kogakuin University, Hachioji 192-0015 Tokyo, Japan*

Hikaru Iiyoshi − *Department of Applied Chemistry, School of Advanced Engineering, Kogakuin University, Hachioji 192-0015 Tokyo, Japan*

Hiromitsu Takaba − *Department of Environmental Chemistry and Chemical Engineering, School of Advanced Engineering, Kogakuin University, Hachioji 192-0015 Tokyo, Japan*

Complete contact information is available at: https://pubs.acs.org/10.1021/acsomega.2c06604

Notes

The authors declare no competing financial interest.

https://doi.org/10.1021/acsomega.2c06604
ACS Omega 2023, 8, 7507−7516

■ ACKNOWLEDGMENTS

This research was supported by the Ministry of Education, Science, Sports and Culture, Grant-in-Aid for Scientific Research (C), 22K04833, 2022−2024.

■ REFERENCES

(1) Tsuji, J. *Palladium in Organic Synthesis*; Springer, 2005.
(2) Okumura, K.; Kobayashi, T.; Tanaka, H.; Niwa, M. Toluene combustion over palladium supported on various metal oxide supports. *Appl. Catal., B* **2003**, *44*, 325−331.
(3) Roy, S.; Hegde, M.; Madras, G. Catalysis for NO_x abatement. *Appl. Energy* **2009**, *86*, 2283−2297.
(4) Lardinois, T. M.; Mandal, K.; Yadav, V.; Wijerathne, A.; Bolton, B. K.; Lippie, H.; Li, C. W.; Paolucci, C.; Gounder, R. Kinetic and Thermodynamic Factors Influencing Palladium Nanoparticle Redispersion into Mononuclear Pd (II) Cations in Zeolite Supports. *J. Phys. Chem. C* **2022**, *126*, 8337−8353.
(5) Priolkar, K.; Bera, P.; Sarode, P.; Hegde, M.; Emura, S.; Kumashiro, R.; Lalla, N. formation of $Ce_{1-x}Pd_xO_{2-\delta}$ solid solution in combustion-synthesized Pd/CeO_2 catalyst: XRD, XPS, and EXAFS investigation. *Chem. Mater.* **2002**, *14*, 2120−2128.
(6) Say, Z.; Dogac, M.; Vovk, E. I.; Kalay, Y. E.; Kim, C. H.; Li, W.; Ozensoy, E. Palladium doped perovskite-based NO oxidation catalysts: The role of Pd and B-sites for NOx adsorption behavior via in-situ spectroscopy. *Appl. Catal., B* **2014**, *154−155*, 51−61.
(7) Liang, H.; Raitano, J. M.; He, G.; Akey, A. J.; Herman, I. P.; Zhang, L.; Chan, S.-W. Aqueous co-precipitation of Pd-doped cerium oxide nanoparticles: chemistry, structure, and particle growth. *J. Mater. Sci.* **2012**, *47*, 299−307.
(8) (a) Kantam, M. L.; Chakravarti, R.; Pal, U.; Sreedhar, B.; Bhargava, S. Nanocrystalline magnesium oxide-stabilized palladium (0): an efficient and reusable catalyst for selective reduction of nitro compounds. *Adv. Synth. Catal.* **2008**, *350*, 822−827. (b) Reddy, P. V.; Annapurna, M.; Srinivas, P.; Likhar, P. R.; Kantam, M. L. Nanocrystalline magnesium oxide-stabilized palladium (0): an efficient and reusable catalyst for synthesis of N-(2-pyridyl) indoles. *New J. Chem.* **2015**, *39*, 3399−3404.
(9) Corma, A.; Ródenas, T.; Sabater, M. J. A Bifunctional Pd/MgO Solid Catalyst for the One-Pot Selective N-Monoalkylation of Amines with Alcohols. *Chem. - Eur. J.* **2010**, *16*, 254−260.
(10) Kantam, M. L.; Roy, S.; Roy, M.; Sreedhar, B.; Choudary, B. Nanocrystalline Magnesium Oxide-Stabilized Palladium (0): An Efficient and Reusable Catalyst for Suzuki and Stille Cross-Coupling of Aryl Halides. *Adv. Synth. Catal.* **2005**, *347*, 2002−2008.
(11) (a) Piccolo, L.; Henry, C. R. NO−CO reaction kinetics on Pd/MgO model catalysts: morphology and support effects. *J. Mol. Catal. A Chem.* **2001**, *167*, 181−190. (b) Prévot, G.; Meerson, O.; Piccolo, L.; Henry, C. Reactivity of supported metal clusters: the reduction of NO by CO on a Pd/MgO (100) model catalyst. *J. Phys.: Condens. Matter* **2002**, *14*, 4251−4269.
(12) (a) Galvagno, S.; Donato, A.; Neri, G.; Pietropaolo, R. Hydrogenation of phenol to cyclohexanone over Pd/MgO. *J. Chem. Technol. Biotechnol.* **2007**, *51*, 145−153. (b) Claus, P.; Berndt, H.; Mohr, C.; Radnik, J.; Shin, E.-J.; Keane, M. A. Pd/MgO: catalyst characterization and phenol hydrogenation activity. *J. Catal.* **2000**, *192*, 88−97.
(13) (a) Goniakowski, J. Electronic structure of MgO-supported palladium films: Influence of the adsorption site. *Phys. Rev. B* **1998**, *57*, 1935−1941. (b) Haas, G.; Menck, A.; Brune, H.; Barth, J.; Venables, J.; Kern, K. Nucleation and growth of supported clusters at defect sites: Pd/MgO (001). *Phys. Rev. B* **2000**, *61*, 11105−11108. (c) Renaud, G.; Barbier, A. Structure and morphology of the Pd/MgO (001) interface during its formation. *Appl. Surf. Sci.* **1999**, *142*, 14−17. (d) Ringleb, F.; Sterrer, M.; Freund, H.-J. Preparation of Pd−MgO model catalysts by deposition of Pd from aqueous precursor solutions onto Ag (001)-supported MgO (001) thin films. *Appl. Catal., A* **2014**, *474*, 186−193.
(14) Heinemann, K.; Osaka, T.; Poppa, H.; Avalos-Borja, M. In situ transmission electron microscope studies of palladium on MgO. *J. Catal.* **1983**, *83*, 61−78.
(15) Gamman, J. J.; Jackson, S. D.; Wigzell, F. A. Synthesis of methyl isobutyl ketone over Pd/MgO/SiO_2. *Ind. Eng. Chem. Res.* **2010**, *49*, 8439−8443.
(16) (a) Kim, H. Y.; Lee, H. M.; Park, J.-N. Bifunctional mechanism of CO_2 methanation on Pd−MgO/SiO_2 catalyst: independent roles of MgO and Pd on CO_2 methanation. *J. Phys. Chem. C* **2010**, *114*, 7128−7131. (b) Kim, H. Y.; Park, J. N.; Henkelman, G.; Kim, J. M. Design of a highly nanodispersed Pd−MgO/SiO_2 composite catalyst with multifunctional activity for CH_4 reforming. *ChemSusChem* **2012**, *5*, 1474−1481.
(17) (a) Narayanan, R.; El-Sayed, M. A. Effect of catalysis on the stability of metallic nanoparticles: Suzuki reaction catalyzed by PVP-palladium nanoparticles. *J. Am. Chem. Soc.* **2003**, *125*, 8340−8347. (b) Uberman, P. M.; Pérez, L. A.; Martín, S. E.; Lacconi, G. I. Electrochemical synthesis of palladium nanoparticles in PVP solutions and their catalytic activity in Suzuki and Heck reactions in aqueous medium. *RSC Adv.* **2014**, *4*, 12330−12341.
(18) Okumura, K.; Amano, J.; Yasunobu, N.; Niwa, M. X-ray absorption fine structure study of the formation of the highly dispersed PdO over ZSM-5 and the structural change of Pd induced by adsorption of NO. *J. Phys. Chem. B* **2000**, *104*, 1050−1057.
(19) Ankudinov, A. L.; Ravel, B.; Rehr, J. J.; Conradson, S. Real-space multiple-scattering calculation and interpretation of x-ray-absorption near-edge structure. *Phys. Rev. B* **1998**, *58*, 7565−7576.
(20) Delley, B. An all-electron numerical method for solving the local density functional for polyatomic molecules. *J. Chem. Phys.* **1990**, *92*, 508−517.
(21) Perdew, J. P.; Burke, K.; Ernzerhof, M. Generalized gradient approximation made simple. *Phys. Rev. Lett.* **1996**, *77*, 3865.
(22) Muller, O.; Roy, R. *Synthesis and Crystal Chemistry of Some New Complex Palladium Oxides*; ACS Publications, 1971.
(23) (a) Peuckert, M. XPS study on surface and bulk palladium oxide, its thermal stability, and a comparison with other noble metal oxides. *J. Phys. Chem. A* **1985**, *89*, 2481−2486. (b) Farrauto, R. J.; Lampert, J. K.; Hobson, M. C.; Waterman, E. M. Thermal decomposition and reformation of PdO catalysts; support effects. *Appl. Catal., B* **1995**, *6*, 263−270.
(24) Penner-Hahn, J. E.X-ray Absorption Spectroscopy. In *Comprehensive Coordination Chemistry II*; Elsevier, 2003; Vol. *2*, pp 159−186.
(25) Koga, K. Electronic and catalytic effects of single-atom Pd additives on the hydrogen sensing properties of Co_3O_4 nanoparticle films. *ACS Appl. Mater. Interfaces* **2020**, *12*, 20806−20823.
(26) Slater, J. C. Atomic radii in crystals. *J. Chem. Phys.* **1964**, *41*, 3199−3204.
(27) Gordon, R. B. *The Structure of Metals and Aloys: By W. Hume-Rothery, RE Smallman and CW Haworth, Published by the Metals and Metallurgy Trust, London*, 5th ed.; Elsevier, 1969.
(28) (a) Otto, K.; Haack, L.; Devries, J. Identification of two types of oxidized palladium on γ-alumina by X-ray photoelectron spectroscopy. *Appl. Catal., B* **1992**, *1*, 1−12. (b) Moroseac, M.; Skála, T.; Veltruská, K.; Matolín, V.; Matolínová, I. XPS and SSIMS studies of Pd/SnO_x system: reduction and oxidation in hydrogen containing air. *Surf. Sci.* **2004**, *566*, 1118−1123.
(29) Kuzmin, A.; Mironova, N.; Purans, J. The influence of Pd mixing and magnetic interactions on the pre-edge peak intensity at the Co (Ni) K absorption edge in solid solutions. *J. Phys.: Condens. Matter* **1997**, *9*, 5277−5286.
(30) Okumura, K.; Hoshi, H.; Iiyoshi, H.; Takaba, H. Formation of a Pt−MgO Solid Solution: Analysis by X-ray Absorption Fine Structure Spectroscopy. *ACS Omega* **2022**, *7*, 27458−27468.
(31) Larimi, A. S.; Kazemeini, M.; Khorasheh, F. Highly selective doped PtMgO nano-sheets for renewable hydrogen production from APR of glycerol. *Int. J. Hydrogen Energy* **2016**, *41*, 17390−17398.

https://doi.org/10.1021/acsomega.2c06604
ACS Omega 2023, 8, 7507−7516

(32) Pilarska, A. A.; Klapiszewski, Ł.; Jesionowski, T. Recent development in the synthesis, modification and application of $Mg(OH)_2$ and MgO: A review. *Powder Technol.* **2017**, *319*, 373−407.
(33) Luo, M.-F.; Hou, Z.-Y.; Yuan, X.-X.; Zheng, X.-M. Characterization study of CeO_2 supported Pd catalyst for low-temperature carbon monoxide oxidation. *Catal. Lett.* **1998**, *50*, 205−209.

https://doi.org/10.1021/acsomega.2c06604
ACS Omega 2023, 8, 7507−7516